Analyst

ROYAL SOCIETY OF CHEMISTRY

PAPER

View Article Online
View Journal | View Issue

Cite this: *Analyst*, 2021, **146**, 7336

Non-enzymatic colorimetric detection of hydrogen peroxide using a μPAD coupled with a machine learning-based smartphone app†

Vakkas Doğan,[a] Elif Yüzer,[b] Volkan Kılıç *[a,c] and Mustafa Şen *[b,d]

In the present study, iodide-mediated 3,3′,5,5′-tetramethylbenzidine (TMB)-H_2O_2 reaction system was applied to a microfluidic paper-based analytical device (μPAD) for non-enzymatic colorimetric determination of H_2O_2. The proposed system is portable and incorporates a μPAD with a machine learning-based smartphone app. A smartphone app called "*Hi-perox Sens*" capable of image capture, cropping and processing was developed to make the system simple and user-friendly. Briefly, circular μPADs were designed and tested with varying concentrations of H_2O_2. Following the color change, the images of the μPADs were taken with four different smartphones under seven different illumination conditions. In order to make the system more robust and adaptive against illumination variation and camera optics, the images were first processed for feature extraction and then used to train machine learning classifiers. According to the results, TMB + KI showed the highest classification accuracy (97.8%) with inter-phone repeatability at t = 30 s under versatile illumination and maintained its accuracy for 10 minutes. In addition, the performance of the system was also comparable to two different commercially available H_2O_2 kits in real samples.

Received 17th October 2021,
Accepted 3rd November 2021

DOI: 10.1039/d1an01888d

rsc.li/analyst

1. Introduction

Hydrogen peroxide (H_2O_2) is considered one of the reactive oxygen species and produced by mammalian cells to mediate a number of physiological processes, including cell proliferation, migration, differentiation and even apoptosis.[1] Even though H_2O_2 is not so reactive, it is able to generate hydroxyl radicals that can attack certain cell components such as DNA and membrane lipids. Changes in its concentration has been associated with the development of various diseases including cancer, Alzheimer and diabetes mellitus.[2,3] It is widely used as disinfectant due to its anti-bacterial and virus activity. It is also a byproduct of oxidases, and therefore its high-sensitive detection is of great importance in developing biosensors for the fields ranging from medical diagnostics to environmental monitoring.[4] Several methods including chemiluminescence, fluorescence, electrochemical and colorimetric, have been proposed to detect H_2O_2 for qualitative and quantitative analysis. Among these methods, colorimetry has been found to be promising due to its cost-efficiency and easy operation. Horseradish peroxidase (HRP) is frequently used in colorimetric sensors where it catalyzes the conversion of a chromogenic agent.[3,5,6] Even though H_2O_2 sensors with HRP offer high sensitivity and selectivity, they suffer from a narrow pH working range, poor reproducibility, high cost and low thermal/chemical stability of the enzyme. To overcome these limitations, researchers are actively studying the catalytic properties of nanomaterials, particularly noble metals and their alloys, to replace enzymes in sensor applications. However, these nanomaterials still suffer from high cost, aggregation and poor stability, and their toxic effects on living things have not been fully investigated.[7,8] Apart from enzymes or nanomaterials, the use of biopolymers with peroxidase like activity or antioxidative activity such chitosan and gelatin have also been reported for the detection of H_2O_2.[7,9]

In addition to the requirements of being sensitive, selective and affordable, H_2O_2 sensors need to be portable, reliable, fast and environmentally friendly that can operate in remote locations or resource-limited settings.[10] In that sense, microfluidic paper-based analytical devices (μPADs) are found to be adequate to meet the requirements, resulting in the development of various types of sensors. Although different methods are used in the fabrication of μPADs, the most preferred method is the one that was first introduced by Whitesides *et al.*[11] The method is based on printing wax patterns that

[a]*Department of Electrical and Electronics Engineering Graduate Program, İzmir Katip Çelebi University, 35620 Turkey. E-mail: volkan.kilic@ikcu.edu.tr; Fax: +90232 325 33 60; Tel: +90 232 329 35 35*
[b]*Department of Biomedical Engineering Graduate Program, İzmir Katip Çelebi University, 35620 Turkey*
[c]*Department of Electrical and Electronics Engineering, İzmir Katip Çelebi University, 35620 Turkey*
[d]*Department of Biomedical Engineering, İzmir Katip Çelebi University, 35620 Turkey. E-mail: mustafa.sen@ikcu.edu.tr*

†Electronic supplementary information (ESI) available. See DOI: 10.1039/d1an01888d

define the microfluidic channels and the boundaries of the detection zone with a solid ink (wax) printer. In μPADs, the concentration of many different analytes can be quantified at the same time based on the intensity variation due to the concentration-dependent color change.[5,12]

In colorimetric analysis, intensity information can be utilized with several color spaces including RGB (Red-Green-Blue), HSV (Hue Saturation-Value), and L*a*b* (Lightness, Green-Red, Blue-Yellow).[13,14] The conventional approach is to derive a calibration curve based on single or multiple channels which leads to the highest correlation between the intensity and concentration (magnitude).[12,15,16] For example, average of R, V and L* was used to obtain the calibration in the quantification of glucose in artificial saliva.[12] The V channel was employed for processing the image to detect the harmful dyes in water[15] while the calibration curve is constructed using R, G, B channels to detect sodium benzoate in foods.[16] Even though the calibration curve performs well in a controlled environment, it has a tendency to deviate in the case of ambient light conditions as the intensity values are sensitive to the illumination sources.[17–19] This problem is handled with sophisticated methodologies like machine learning which has emerged as a powerful tool for classification problems due to its flexibility and adaptability to dynamic conditions based on the features extracted from colorimetric information.[5,20–23] The alcohol level in saliva was detected using features of four color spaces (RGB, HSV, YUV and L*a*b*) under three machine learning classifiers[21] while lead ion concentration was estimated with only RGB values.[22] The peroxide concentration was quantified with color features in machine learning classifiers[20] while the glucose concentration was determined with different reagents using color and texture features.[5] Mølgaard *et al.*[24] also employed machine learning approach to detect the H_2O_2 using colorimetric sensor technology for air-sampling. One benefit of machine learning is to be compatible with smartphone apps which offers to perform colorimetric analysis in the field without extensive training.[25] The *GlucoSensing* app was developed to determine the glucose concentration[5] while the *ChemTrainer* app was used to detect peroxide according to the color changes in the colorimetric test strips.[20] *SPAQ2* app was developed to test the alcohol level in saliva.[21] A custom app was developed to predict lead ion.[22] All these apps provide user-friendly interfaces to perform colorimetric analysis with machine learning.

In this study, non-enzymatic μPADs coupled with a machine learning-based smartphone app were developed for high-sensitive and selective determination of H_2O_2 in transparent liquids such as water. First, circular patterns were printed on a filter paper using a wax printer, and then the patterns were processed at high temperature to obtain hydrophobic boundaries of the μPADs. The use of single or multiple indicators have been reported for the colorimetric detection of H_2O_2 such as 3,3′-diaminobenzidine, 3,3′,5,5′-tetramethylbenzidine (TMB), potassium iodide (KI), 4-aminoantipyrine (4-AAP)/3,5-dichloro-2-hydroxy-benzenesulfonic acid, 4-AAP/*N*-ethyl-*N*-(3-sulfopropyl)-3-methylaniline sodium salt, 2,4,6-tribromo-3-hydroxy benzoic acid.[26–29] The μPADs were prepared for testing by adding only two indicators, TMB and KI, to the detection zones (Fig. 1). No enzyme or nanoparticle with catalytic properties were used for the detection, making the system cost-efficient and chemically/thermally stable. The performance of the system was compared with those of using KI only and TMB only. In order to make the process more user friendly, robust and adaptive against illumination variation and camera optics, a machine learning-based smartphone app with a simple interface was developed. Machine learning classifiers were trained using features extracted from images taken under seven different illumination conditions. The trained classifiers were then integrated into the *Hi-perox Sens* app to be presented to the user. The results clearly showed that the proposed system has high potential for practical use.

2. Materials and methods

2.1. Materials

Potassium chloride (KCl) (Sigma Aldrich, USA), TMB (Sigma Aldrich, USA), potassium iodide (KI) (Sigma Aldrich, USA),

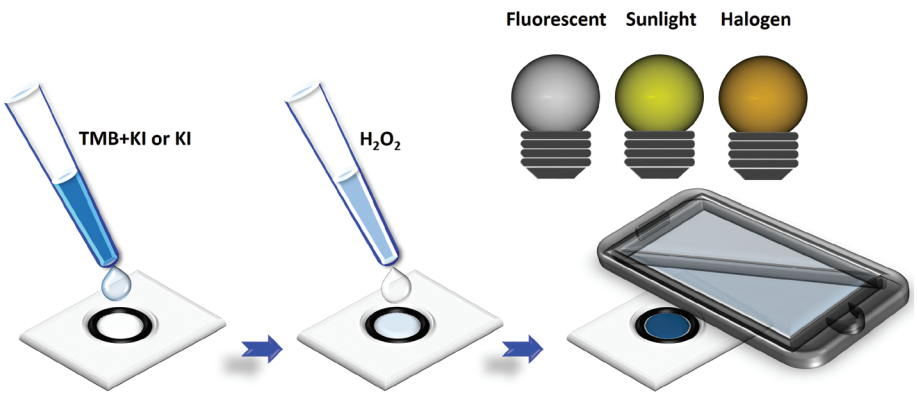

Fig. 1 Schematic illustration of the proposed system. The color change of chromogenic agents can be detected with a smartphone camera under ambient light conditions.

sodium chloride (NaCl) (Sigma Aldrich, USA), calcium chloride $CaCl_2$ (Sigma Aldrich, USA), H_2O_2 (Sigma Aldrich, USA), D (+)-glucose ($C_6H_{12}O_6$) ≥ 99.5%, sucrose (Sigma Aldrich, USA), lactate (Sigma Aldrich, USA), urea (Sigma Aldrich, USA), Whatman qualitative filter paper-grade 1 (Sigma Aldrich, USA). All chemicals were used as received and prepared using MilliQ-water throughout the study.

2.2. μPAD fabrication and colorimetric detection of H_2O_2

First, a circular design to be used as a reaction/detection zone of μPADs was drawn in Microsoft PowerPoint. This design was then printed on a Whatman filter paper with a wax printer. In general, solid ink is a mixture of hydrocarbons and hydrophobic carbamates with a melting point of about 120 °C. After printing, the solid ink was kept on a heater at approximately +150 °C for 3 minutes. An aluminum foil and a planar weight (1–2 kg) were placed on top of the paper to ensure uniform heat transfer from the hot plate to the paper and penetration of the melted solid ink into the pores of the chromatography paper. Hence, solid ink boundaries that define the reaction/detection zone were obtained. Next, three different μPADs were prepared by introducing 0.8 μl KI (6 M), TMB (10 mM) + KI (6 M) and TMB (10 mM) into μPADs, respectively. The μPADs were left to dry for about 5 minutes in order for the liquids to dry. Next, the μPADs were tested for the colorimetric detection of H_2O_2 at varying concentrations (0.01, 0.05, 0.1, 0.2, 0.5, 1, 5, 10, 25, 50 mM), in which case 2 μL aliquots of test solutions were introduced into the reaction/detection zones of μPADs. The image of each μPAD was captured using a smartphone camera at t = 30 s and t = 10 min, respectively.

2.3. Data acquisition and processing

Machine learning classifiers need to be trained with a dataset that has a strong representation of all possible conditions in order to get a significant classification performance.[30,31] The robustness and adaptability of the system, therefore, are highly dependent on the dataset which needs to be enlarged considering illumination conditions and camera optics. To address these issues, the images of the μPAD were captured with multiple smartphones under halogen (H), fluorescent (F), and sunlight (S) light bulb sources to imitate the conditions. The halogen bulb emits 2700 K warm colors while the fluorescent and sunlight bulbs give 4000 K neutral and 6500 K cool colors, respectively. Three light sources were used to get seven light conditions including H, F, S, HF, HS, FS, HFS, running single or multiple light sources together. The bulb sources were located 50, 53, and 57 cm away from H, F, and S, respectively. In addition, the capturing was performed at an incidence angle of 30° under a homogeneously illuminated area with a constant distance of 8 cm between the smartphone and the μPAD.

To maintain inter-phone operability, four different smartphones with different brands (Oppo A5 2020, Reeder P10, iPhone 5SE, and iPhone 6S) and operating systems (Android and iOS) were used for capturing. The specifics of cameras for each smartphone are shown in Table 1. Images were captured in automatic mode at t = 30 s and t = 10 min as shown in Fig. 2. 28 images were taken with each smartphone separately under seven different illumination conditions at two-time steps, resulting in fifty-six images. Since the group of eleven concentrations was captured at a single frame, 616 images of each concentration were collected for TMB + KI and KI, respectively. These images were, then, transferred to a computer to process in MATLAB (MathWorks, MA, USA) environment for feature extraction.

2.4. Feature extraction and machine learning analysis

Feature extraction is identifying an object based on properties such as size, shape, composition, and location of the object.[32] In mathematical terms, it is the process of inferring from raw data information to increase the variability of the class pattern while minimizing the in-class pattern variability which facilitates quantitative measurements, classification, and object identification.[33] The feature extraction is a crucial step in the visual inspection as it has an observable effect on the efficiency of the machine learning classifiers. Before training the classifiers, image features were extracted based on color and texture information. The region of interest (ROI) for each concentration was cropped to convert the RGB image into HSV and L*a*b*, resulting in a total of 9 color channel (R, G, B, H, S, V, L*, a*, b*) information. Then, the mean, skewness and kurtosis values were calculated for each color channel which leads to 27 features. As a texture features, contrast, correlation, homogeneity, and energy were also extracted.[34,35] In addition to the color and texture features, the entropy and intensity values were also added to have a total of 33 features.

Table 1 The smartphones used to create a dataset with images of μPADs for machine learning

Smartphone brand	Image resolution	Optics	Camera resolution
iPhone 5SE	4032 × 3024	*f*/2.2	7 MP
iPhone 6S	4032 × 3024	*f*/2.2	12 MP
Oppo A5 2020	4000 × 3000	*f*/1.8	12 MP
Reeder P10	4160 × 3120	*f*/2	13 MP

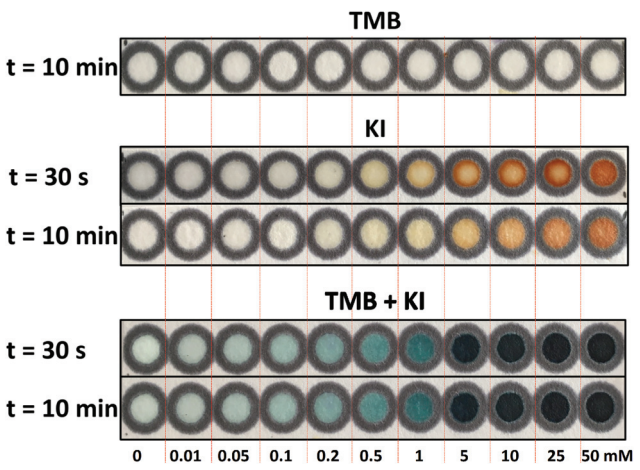

Fig. 2 Color changes with respect to chromogenic agents, time and concentrations.

To determine the H_2O_2 based on color changes, twenty-three machine learning classifiers were trained with the extracted features and their performances were compared in terms of classification accuracy. Among these classifiers, linear discriminant analysis (LDA) and ensemble bagging classifier (EBC) outperformed the others for KI and TMB + KI, respectively. The LDA is a kind of supervised classifier which applies Bayesian and maximum likelihood rules to estimate the highest likelihood between input and pre-defined classes using discriminant function.[36] In maximum likelihood rule, input x is assigned to class j,

$$j = \underset{i}{\operatorname{argmax}} f_i(x), \quad (1)$$

under the assumption that each class may exist with equal probability. Here, $f_i(x)$ denotes the class density. However, if the class prior probabilities, π, is known, x is assigned to class j

$$j = \underset{i}{\operatorname{argmax}}\, \pi_i f_i(x). \quad (2)$$

EBC is an ensemble technique used to improve the performance of machine learning classifiers in terms of stability and accuracy. It combines the classifications of randomly generated training sets in the estimation of the final prediction[37] based on bagging algorithm of which the pseudo code is given in Algorithm 1. The samples are generated with bootstrap methods from the training set S uniformly. The generated T bootstrap samples builds C_i classifiers (C_1, C_2, ...C_T) which are used to estimate the final classifier, C^*.[38]

Algorithm 1: The bagging algorithm

Inputs: training set S, inducer I, integer T
for $i = 1$ to T do

$S' =$ bootstrap sample from S
$C_i = I(S')$

end
$C^*(x) = \operatorname{argmax}_{y \in Y} \sum_{i=C_i(x)}^{y} 1$

Output: classifier C^*

Here, y denotes the class label from a discrete space Y associated with x for a given instance.

As the LDA and EBC showed the best classification performance, they were integrated into our smartphone application called *Hi-perox Sens*.

2.5. Smartphone app: *Hi-perox Sens*

Our custom-designed Android app, *Hi-perox Sens*, was developed for quantitative evaluation of H_2O_2 in μPADs with machine learning, enabling colorimetric analysis operable whenever or wherever needed. The LDA and EBC machine learning classifiers, running in the remote server, were integrated into the *Hi-perox Sens* due to their outstanding performances. The *Hi-perox Sens* uses a Firebase cloud system for both transferring the image to the remote server, and receiving the classification result back to the app.

With a simple and user-friendly interface, *Hi-perox Sens* is demonstrated in Fig. 3. The homepage is given in Fig. 3(a) where an image can be taken from the gallery of the smartphone (Fig. 3(b)) or a new image can be captured using the smartphone camera. Once the image is selected or captured, it is displayed on the app as shown in Fig. 3(c). Next, the ROI on the image needs to be drawn using an adjustable crop box as shown in Fig. 3(d and e). Then, the ROI is cropped and displayed on the app (Fig. 3(f)) to double-checked the ROI whether the selected area is suitable for the analysis. If not, the ROI can be re-drawn before the cropped patch is transferred to the remote server *via* a Firebase by tapping the upload icon. Machine learning classifiers running in the remote server quantify the concentration level. As shown in Fig. 3(g), the colorimetric reagent information (TMB + KI or KI) also needs to be sent to the remote server in order to choose the best classifier for the colorimetric analysis. Last, the result is sent back to *Hi-perox Sens via* a Firebase to display on the app (Fig. 3(h)).

2.6. Selectivity

The selectivity of the μPADs towards H_2O_2 was tested with a number of interfering species including KCl (2 mM), NaCl (2 mM), $CaCl_2$ (2 mM), sucrose (2 mM), urea (2 mM) and lactate (2 mM). Briefly, 2 μL aliquots of interfering and test solutions were introduced into the reaction/detection zones of different μPADs, respectively. The image of each μPAD was captured using a smartphone camera at t = 10 min and analyzed based on RGB intensity data.

2.7. Determination of H_2O_2 in real samples

Tap water was taken directly from the tap, and milk was purchased from a local market. Prior to analysis, milk was diluted a hundredfold using deionized water to reduce matrix effect. Two commercially available products were used to evaluate the performance of the present system: (i) H_2O_2 Colorimetric Assay Kit (Sigma-Aldrich, USA) and (ii) Quantofix® peroxide 100 semi-quantitative test strips (Macherey-Nagel, Germany). After testing the real samples as prepared, they were spiked by adding varying concentrations of H_2O_2 (0, 0.01, 0.025, 0.05, 0.1, 0.2, 0.5, 1, 5 mM). Measurements were performed as specified in the product manual and the results were compared with those of the current system.

3. Results and discussion

Here, iodide-mediated TMB-H_2O_2 reaction system was used instead of an enzyme or a nanomaterial with catalytic properties for the detection of H_2O_2. Briefly, three different chromogenic agent mixtures were tested with varying concentrations of H_2O_2; (i) only TMB, (ii) only KI and (iii) TMB + KI. As can be seen in Fig. 2, no color change was observed in the case of only TMB, which clearly demonstrates that TMB by itself cannot catalyze the oxidation of H_2O_2. However, in the case of only KI, H_2O_2 catalyzes the conversion of KI to iodine and hence producing a visual brownish color. Although the

Fig. 3 Colorimetric hydrogen peroxide quantification steps on the *Hi-perox Sens*. The homepage of the *Hi-perox Sens* is given in (a). The user can select an image from the gallery or capture a new image using the smartphone camera in (b) and display it on the screen as in (c). The image can be cropped using an adjustable crop box in (d). The cropped patch is given in (e) and uploading the cropped patch is shown in (f). The user selection of the uploading patch as TMB + KI or KI is shown in (g). The classification result of the image is given in (h).

changing color intensity was not proportional to the low concentration of H_2O_2, a linear correlation was observed when the H_2O_2 concentration exceeded 1 mM level (Fig. 2). When TMB + KI was used as the detection mixture, a blue color appeared in the presence of H_2O_2. The color change was clearly caused by the oxidation of TMB. A possible chemical reaction equation involving three steps was presented below.

$$2KI + H_2O_2 \rightleftharpoons I_2 + 2KOH \quad (3)$$

$$I_2 + 5H_2O_2 \rightleftharpoons 2HIO_3 + 4H_2O \quad (4)$$

$$\text{red-TMB} + IO_3^- + 6H^+ \rightleftharpoons \text{ox-TMB} + I^- + 3H_2O \quad (5)$$

In the first step (eqn (3)), KI gets into a reaction with H_2O_2 and produces I_2, which is then once again reacts with H_2O_2 to produce iodic acid (HIO_3) (eqn (4)). As HIO_3 ionizes, iodate (IO_3^-) is formed. In the final stage (eqn (5)), the oxidation of TMB is induced by the reduction of IO_3^- to I^-, resulting in the formation of blue color. According to this reaction, iodide serves as a catalyst for the rapid oxidation of TMB. Unlike the chromogenic agent KI, TMB + KI performed best in the low concentration range of H_2O_2, and the color intensity became saturated when the H_2O_2 concentration level exceeded 5 mM (Fig. 2). In addition, the effect of pH and ionic strength on the signal response of μPADs were tested in the presence of 1 mM H_2O_2. In the pH range of 5 to 11, no significant change in color formation was observed. However, the intensity of the color formed at pH 3 was lower than the rest (ESI Fig. S1†). As for the ionic strength, it appears that the color intensity slightly increased with increasing NaCl concentration. The

adopted strategy has the potential to provide an important basis for simple, rapid, cost-effective, sensitive and selective colorimetric assay for the detection of H_2O_2.

In this study, H_2O_2 concentration was detected using machine learning classifiers based on the color change that occurred in the μPADs. Machine learning classifiers need to be trained in advance with a dataset which contains similar images that the user might use in testing. Therefore, the dataset was created with four different smartphones (iPhone 5SE, iPhone 6S, Oppo A5 2020, and ReederP10) under seven illumination conditions (H, F, S, HF, HS, FS, HFS). This dataset was transferred to a computer for pre-processing in MATLAB 2021b. The ROI for each concentration was cropped to extract features for the training of machine learning classifiers. First, twenty-three classifiers were trained for TMB + KI and KI with eleven concentrations ranging from 0 to 50 mM at t = 30 s. The best classification results were 81.3% and 91.9% for KI and TMB + KI, respectively. After careful analysis of confusion matrices of the classifiers, it was observed that KI and TMB + KI failed to classify H_2O_2 in lower and higher concentrations ranges, respectively. Therefore, classifiers were trained again with low concentration values (0, 0.01, 0.05, 0.1, 0.2, 0.5, 1, 5 mM) for TMB + KI, and high concentration values (0, 0.2, 0.5, 1, 5, 10, 25, 50 mM) for KI. As a result, the classification accuracies were improved to 97.3% and 92.4% for TMB + KI and KI, respectively. These results were summarized in Table 2. The same process was repeated with images taken at t = 10 min, and the results were given in Table 3. The system shows similar classification accuracy even after 10 min which proves the robustness of the system.

In classification, the EBC gave the highest accuracy for TMB + KI while the LDA outperformed for KI. Besides the classification accuracy (eqn (6)), the performance of these classifiers was also tested in terms of precision (eqn (7)), recall (eqn (8)), and F1 score (eqn (9)).

$$\text{Accuracy} = \frac{\text{TP} + \text{TN}}{\text{TP} + \text{TN} + \text{FP} + \text{FN}}, \quad (6)$$

$$\text{Precision} = \frac{\text{TP}}{\text{TP} + \text{FP}}, \quad (7)$$

$$\text{Recall} = \frac{\text{TP}}{\text{TP} + \text{FN}}, \quad (8)$$

$$\text{F1 score} = 2 \times \frac{\text{Precision} \times \text{Recall}}{\text{Precision} + \text{Recall}}, \quad (9)$$

TP (True Positive) describes the number of predictions that are positive, and also classified as positive by the classifier. FP (False Positive) is the number of predictions that were positive but were not classified as positive by the classifier. TN (True Negative) indicates the number of predictions that are also classified as negative by the classifier. FN (False Negative) is the number of predictions that are negative but not classified as negative by the classifier.[39] Accuracy is the most commonly used metric in the classification comparison. It is the ratio of correctly classified samples to the total number of samples. Precision is the ratio of the number of samples labeled as positive to the total samples classified as positive. Sensitivity is the ratio of positively labeled samples to the total number of truly positive samples. The F1 score is calculated using precision and sensitivity metrics. It is used to optimize the system towards precision or sensitivity. As can be seen the performance metrics results (Fig. 5), TMB + KI had the highest accuracy value with 97.8% using EBC. The detailed classification reports and confusion matrices with respect to the type of chromogenic agents, timing and concentration range can be found in ESI Tables S1–8 and ESI Fig. S2–12.†

It should be noted that the performance metric results were lower than the average values in the cases of 0.01 and 0.05 mM H_2O_2. This can also be observed in the confusion matrix shown in Fig. 4(a), visualizing the performance metrics. Confusion matrix is mostly used to illustrate the relation between the true and predicted outputs of the classifier concerning each class. Robustness of the system can be easily and visually observed when the confusion matrices of TMB + KI at 30 s (Fig. 4(a)) and 10 min (Fig. 4(b)) were compared. Fig. 4(c) and (d) show performance analysis of LDA for KI at 30 s and 10 min, respectively. According to the matrices, much better prediction accuracy and robustness were achieved in high concentration range of H_2O_2, as in TMB + KI.

Finally, in our study, LDA and EBC classifiers were integrated with *Hi-perox Sens*, which is a simple and user-friendly mobile app for H_2O_2 detection. Images of this app are shown in Fig. 3. The photo is selected from the gallery or captured using the camera, then the ROI is cropped and sent *via* Firebase to the remote server running the machine learning classifier to measure the concentration level. The result is then returned and displayed in *Hi-perox Sens*. As an example, the processes performed on an uploaded image are shown step by step in Fig. 3. At last, *Hi-perox Sens* correctly classified the H_2O_2 concentration as 25 mM. The smartphone-based system successfully worked and quantified H_2O_2 level in water with machine learning classifiers. The LOD of the sensor with TMB + KI was calculated to be 5.4 μM based on the RGB data of images taken under HFS with iPhone 6S (LOD = 3.3 × σ/slope). Although the system works without a calibration curve, the calculated LOD

Table 2 The classification results at t = 30 s for TMB + KI and KI

H_2O_2 concentration	0–50 mM	High	Low
KI	81.3	92.3	—
TMB + KI	91.9	—	97.8

Table 3 The classification results at t = 10 min for TMB + KI and KI

H_2O_2 concentration	0–50 mM	High	Low
KI	89.1	92.4	—
TMB + KI	85.1	—	97.3

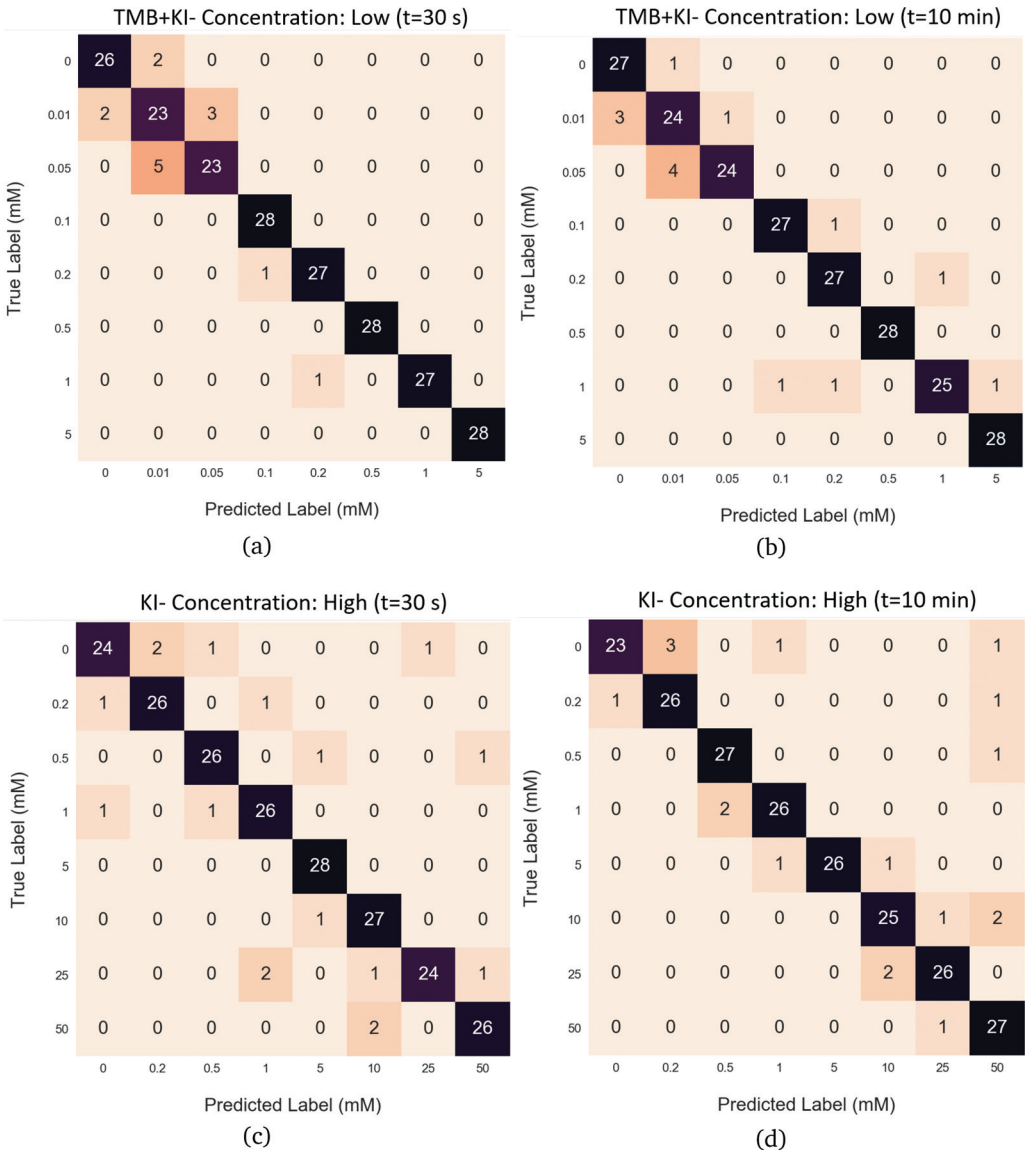

Fig. 4 Confusion matrices of TMB + KI for the EBC classifier at t = 30 s are given in (a) and at t = 10 min in (b), and confusion matrices of KI for the LDA classifier at t = 30 s are shown in (c) and at t = 10 min in (d).

value clearly demonstrates its potential to be trained for lower concentrations of H_2O_2. Additionally, the selectivity of the μPAD towards H_2O_2 was tested in the presence of a number of interfering species such as KCl (2 mM), NaCl (2 mM), $CaCl_2$ (2 mM), sucrose (2 mM), urea (2 mM) and lactate (2 mM) (n = 3). As can be seen in Fig. 6, the μPAD did not respond to any of the interfering molecules as the difference between the control and test groups was not significant. In other words, the μPAD was able to selectively measure H_2O_2 concentration, further proving the robustness of the proposed system.

The most relevant studies include,[20,24,40,41] which, however, still substantially differ from the present study. First of all, either enzymes or catalytic nanoparticles were used in these papers to induce color change in the presence of H_2O_2. On the contrary, here, iodide-mediated TMB-H_2O_2 reaction system was applied to μPADs for non-enzymatic H_2O_2 quantification, which made the system low-cost. In addition, unlike Cheng *et al.*[40] and Bandi *et al.*,[41] where a calibration curve based colorimetric H_2O_2 detection was performed, our proposed system is based on machine learning, offering more robustness and adaptability against ambient illumination conditions and camera optics. Solmaz *et al.*[20] and Molgaard *et al.*[24] also employed the machine learning classifiers and reported that H_2O_2 was detected with 95% accuracy in both studies. Therefore, the proposed system is clearly state-of-the-art performance in terms of robustness, adaptability and classification accuracy. To verify the practical applicability of the present system, its performance was compared to two commercially available products in tap and milk samples. As can be seen from Table 4, promising and acceptable recovery of H_2O_2

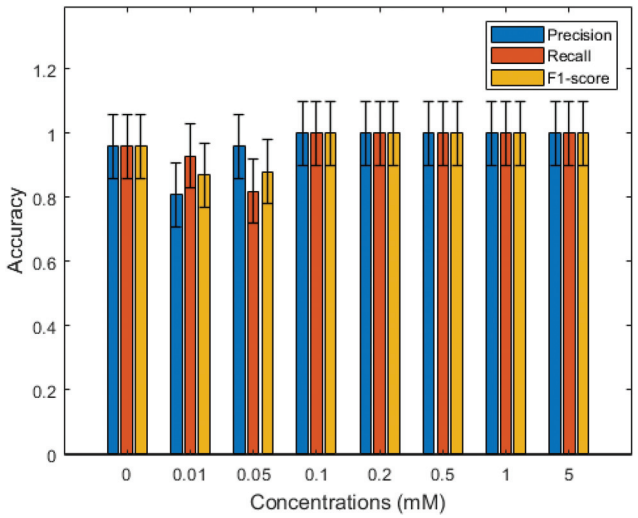

Fig. 5 Evaluation of EBC with error bars in terms of precision, recall, and F1 score at t = 30 s for TMB + KI using low concentrations of H_2O_2.

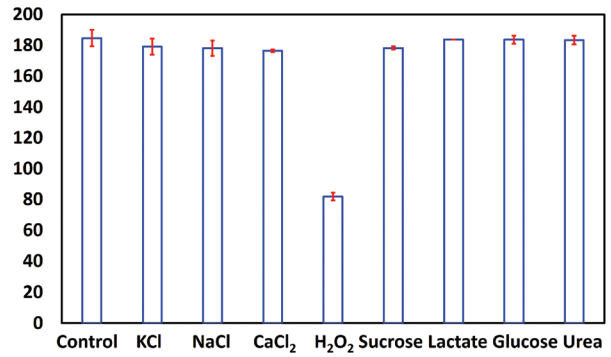

Fig. 6 Selectivity test for the proposed system.

in real samples was obtained with the present system. Although it had a slightly lower recovery (89.4% at t = 30 s and 81% at t = 10 min, in average) than the commercially available H_2O_2 Colorimetric Assay Kit (105.5% in average), the system showed a much better recovery in milk (92.5%). The matrix effect of milk adversely affected the results of the H_2O_2 Colorimetric Assay Kit (162.4%), where the analysis was performed with a UV spectrophotometer. Quantofix® peroxide test is an enzyme-based assay used to visually determine the H_2O_2 concentration in a given sample. Since visual observation is prone to error, ImageJ was used to determine the exact interval of H_2O_2 according to the color scale given on the product. Although the test strips accurately determined the concentration interval of H_2O_2 in tap water, they misclassified 0.2 mM of H_2O_2 in milk. Normally, test strips require a reflectometer (test stripreader) for both quantitative analysis and to eliminate the subjectivity of visual reading. As a result, the proposed system had comparable performance in real samples to two commercially available H_2O_2 kits. Although not done in this study, it should be noted that the accuracy of the system can be significantly improved by including real samples in the machine learning classifier training dataset.

4. Conclusion

Here, iodide-mediated TMB-H_2O_2 (TMB + KI) reaction system was applied for high sensitive, selective and accurate non-enzymatic colorimetric determination of H_2O_2 in transparent liquids such as water using a μPAD coupled with a machine learning based smartphone app. The results were analyzed by comparison with those of KI. The reaction of H_2O_2 and chromogenic agents (TMB + KI or KI) in μPADs led to a concentration-dependent color change without requiring any enzymes or catalytic nanoparticles. To the best of our knowledge, this is the first study that links a machine learning based smartphone app with chromogenic agents in μPADs, enabling non-enzymatic quantitative analysis of H_2O_2 for rapid and portable on-site surveillance. To ensure the system works independently of camera optics and ambient light conditions, the dataset was created with four different smartphones in seven different illumination conditions for the training of machine learning classifiers. Based on performance comparison of various machine

Table 4 Real sample analysis for the determination of H_2O_2 in tap water and milk samples

		Hi-perox Sens (t = 30 s)		Hi-perox Sens (t = 10 min)	Peroxide assay kit		Quantofix	
Real samples	Added (mM)	Found[a] (mM)	Recovery	Found[a] (mM)	Recovery	Found (mM)	Recovery	Interval
Tap water	0	0	—	0	—	−0.008571	—	<0.3
	0.2	0.32	57.2	0.14	71.4	0.1628571	81.5	0.1–0.3
	0.5	0.5	100	0.5	100	0.6057143	121	0.3–0.9
	1	1	100	1.57	63.7	1.1819048	118.2	0.9–3
	5	5	100	4.43	88.6	5.0628571	101.3	>3
Milk	0	0	—	0	100	0.2819048	—	<0.3
	0.2	0.14	71.4	0.14	71.4	0.5104762	255.2	0.3–0.9
	0.5	0.5	100	0.5	100	0.8009524	160.2	0.3–0.9
	1	1	100	1	100	1.3961905	139.61	0.9–3
	5	5	100	5	100	4.7295238	94.5	>3

[a] The average of classification results.

learning classifiers, TMB + KI gave the highest classification accuracy (97.8%) in the 0 to 5 mM concentration range, whereas KI performed its best between 0.2 and 50 mM with 92.3% accuracy. These results indicated that in the quantitative analysis of H_2O_2, KI performs better in the high concentration range, while TMB + KI is more efficient in the low range. The system could be further extended by enlarging the dataset for closer concentration levels and employing more sophisticated methodologies such as deep learning and transfer learning to improve classification accuracy and sensitivity. Overall, the proposed system offers the advantages of portability, rapid response, easy operation, high selectivity and can be applied in point-of-care sensing, healthcare and environmental monitoring in resource-limited settings.

Conflicts of interest

There are no conflicts to declare.

References

1 S. G. Rhee, *Science*, 2006, **312**, 1882–1883.
2 S. Bocanegra-Rodríguez, N. Jornet-Martínez, C. Molins-Legua and P. Campíns-Falcó, *ACS Omega*, 2020, **5**, 2419–2427.
3 F. Behrouzifar, S.-A. Shahidi, F. Chekin, S. Hosseini and A. Ghorbani-HasanSaraei, *Spectrochim. Acta, Part A*, 2021, **257**, 119761.
4 J. E. Giaretta, F. Oveissi, F. Dehghani and S. Naficy, *Adv. Mater. Technol.*, 2021, **6**, 2001148.
5 Ö. B. Mercan, V. Kılıç and M. Şen, *Sens. Actuators, B*, 2021, **329**, 129037.
6 Q. Wang, R. Xue, H. Guo, Y. Wei and W. Yang, *J. Electroanal. Chem.*, 2018, **817**, 184–194.
7 K. Ragavan, S. R. Ahmed, X. Weng and S. Neethirajan, *Sens. Actuators, B*, 2018, **272**, 8–13.
8 X. Xiong, C. You, X. Cao, L. Pang, R. Kong and X. Sun, *Electrochim. Acta*, 2017, **253**, 517–521.
9 M.-M. Liu, X. Lian, H. Liu, Z.-Z. Guo, H.-H. Huang, Y. Lei, H.-P. Peng, W. Chen, X.-H. Lin, A.-L. Liu, *et al.*, *Talanta*, 2019, **200**, 511–517.
10 N. Jiang, N. D. Tansukawat, L. Gonzalez-Macia, H. C. Ates, C. Dincer, F. Guder, S. Tasoglu and A. K. Yetisen, *ACS Sens.*, 2021, 2108–2124.
11 A. W. Martinez, S. T. Phillips, M. J. Butte and G. M. Whitesides, *Angew. Chem.*, 2007, **119**, 1340–1342.
12 T. Golcez, V. Kilic and M. Sen, *Anal. Sci.*, 2021, **37**(4), 561–568.
13 Ö. B. Mercan and V. Kılıç, *International Conference on Intelligent and Fuzzy Systems*, 2020, pp. 1276–1283.
14 A. Kökten and V. Kılıç, *Eur. J. Sci. Technol.*, 2021, 68–72.
15 G. Kocakusak, A. Bayram, V. Kilic, N. Horzum and M. Solmaz, *Anal. Methods*, 2017, **9**, 579–585.
16 C.-H. Ko, C.-C. Liu, K.-H. Chen, F. Sheu, L.-M. Fu and S.-J. Chen, *Food Chem.*, 2021, **345**, 128773.
17 V. Kiliç and M. Şen, *2019 Medical Technologies Congress (TIPTEKNO)*, 2019, pp. 1–4.
18 T. Gölcez, V. Kiliç and M. Şen, *2019 Medical Technologies Congress (TIPTEKNO)*, 2019, pp. 1–4.
19 Ö. Kap, V. Kılıç, J. G. Hardy and N. Horzum, *Analyst*, 2021, **146**, 2784–2806.
20 M. E. Solmaz, A. Y. Mutlu, G. Alankus, V. Kilic, A. Bayram and N. Horzum, *Sens. Actuators, B*, 2018, **255**, 1967–1973.
21 H. Kim, O. Awofeso, S. Choi, Y. Jung and E. Bae, *Appl. Opt.*, 2017, **56**, 84–92.
22 S. Sajed, M. Kolahdouz, M. A. Sadeghi and S. F. Razavi, *ACS Omega*, 2020, **5**, 27675–27684.
23 F. Cui, Y. Yue, Y. Zhang, Z. Zhang and H. S. Zhou, *ACS Sens.*, 2020, **5**, 3346–3364.
24 L. L. Mølgaard, O. T. Buus, J. Larsen, H. Babamoradi, I. L. Thygesen, M. Laustsen, J. K. Munk, E. Dossi, C. O'Keeffe and L. Lässig, *et al.*, *Chemical, Biological, Radiological, Nuclear, and Explosives (CBRNE) Sensing XVIII*, 2017, p. 1018307.
25 B. R. Sun, A. G. Zhou, X. Li and H.-Z. Yu, *ACS Sens.*, 2021, **6**, 1731–1744.
26 W.-J. Zhu, D.-Q. Feng, M. Chen, Z.-D. Chen, R. Zhu, H.-L. Fang and W. Wang, *Sens. Actuators, B*, 2014, **190**, 414–418.
27 D. M. Cate, W. Dungchai, J. C. Cunningham, J. Volckens and C. S. Henry, *Lab Chip*, 2013, **13**, 2397–2404.
28 E. F. Gabriel, P. T. Garcia, T. M. Cardoso, F. M. Lopes, F. T. Martins and W. K. Coltro, *Analyst*, 2016, **141**, 4749–4756.
29 A. Fang, Q. Wu, Q. Lu, H. Chen, H. Li, M. Liu, Y. Zhang and S. Yao, *Biosens. Bioelectron.*, 2016, **86**, 664–670.
30 Ö. B. Mercan, *et al.*, *2020 Medical Technologies Congress (TIPTEKNO)*, 2020, pp. 1–4.
31 Ö. B. Mercan, V. Doğan and V. Kılıç, *2020 Medical Technologies Congress (TIPTEKNO)*, 2020, pp. 1–4.
32 M. Nixon and A. Aguado, *Feature extraction and image processing for computer vision*, Academic press, 2019.
33 D. P. Tian, *et al.*, *Int. J. Multimedia Ubiquitous Eng.*, 2013, **8**, 385–396.
34 U. E. Yildiz and V. Kiliç, *2019 Medical Technologies Congress (TIPTEKNO)*, 2019, pp. 1–4.
35 A. Y. Mutlu and V. Kılıç, 26th Signal Processing and Communications Applications Conference (SIU), 2018, pp. 1–4.
36 Z. Fan, Y. Xu and D. Zhang, *IEEE Trans. Neural Netw. Learn. Syst.*, 2011, **22**, 1119–1132.
37 S. Sreng, N. Maneerat, K. Hamamoto and R. Panjaphongse, *Appl. Sci.*, 2018, **8**, 1198.
38 E. Bauer and R. Kohavi, *Mach. Learn.*, 1999, **36**, 105–139.
39 T. J. Lawrence, D. L. Carper, M. K. Spangler, A. A. Carrell, T. A. Rush, S. J. Minter, D. J. Weston and J. L. Labbé, *Bioinformatics*, 2021, **37**, 2058–2060.
40 Y. Cheng, L. Liang, F. Ye and S. Zhao, *Biosensors*, 2021, **11**, 204.
41 R. Bandi, M. Alle, C.-W. Park, S.-Y. Han, G.-J. Kwon, N.-H. Kim, J.-C. Kim and S.-H. Lee, *Sens. Actuators, B*, 2021, **330**, 129330.

